

ORYX MLLM: ON-DEMAND SPATIAL-TEMPORAL UNDERSTANDING AT ARBITRARY RESOLUTION

Anonymous authors

Paper under double-blind review

ABSTRACT

Visual data comes in various forms, ranging from small icons of just a few pixels to long videos spanning hours. Existing multi-modal LLMs usually standardize these diverse visual inputs to fixed-resolution images or patches for visual encoders and yield similar numbers of tokens for LLMs. This approach is non-optimal for multimodal understanding and inefficient for processing inputs with long and short visual contents. To solve the problem, we propose Oryx, a unified multimodal architecture for the spatial-temporal understanding of images, videos, and multi-view 3D scenes. Oryx offers an on-demand solution to seamlessly and efficiently process visual inputs with arbitrary spatial sizes and temporal lengths through two core innovations: 1) a pre-trained OryxViT model that can encode images at any resolution into LLM-friendly visual representations; 2) a dynamic compressor module that supports 1x to 16x compression on visual tokens by request. These designs enable Oryx to accommodate extremely long visual contexts, such as videos, with lower resolution and high compression while maintaining high recognition precision for tasks like document understanding with native resolution and no compression. Beyond the architectural improvements, enhanced data curation and specialized training on long-context retrieval and spatial-aware data help Oryx achieve strong capabilities in image, video, and 3D multimodal understanding simultaneously.

1 INTRODUCTION

Multi-Modal Large Language Models (MLLMs) have made significant strides in processing and integrating visual and linguistic inputs to generate coherent and contextually relevant responses. Proprietary models such as (OpenAI, 2023b; 2024; GeminiTeam, 2024) exemplify the cutting-edge capabilities of MLLMs. Concurrently, the open-source community is actively advancing MLLMs by enhancing their ability to understand diverse visual content (Tong et al., 2024; Liu et al., 2024g; Yang et al., 2023a), including images (Li et al., 2024a; Chen et al., 2024b), videos (Lin et al., 2023a; Cheng et al., 2024; Qian et al., 2024), and 3D data (Hong et al., 2023), *etc.* As MLLMs become stronger, there is a growing need for more general and unified MLLMs that are capable of processing visual content in more diverse forms and accomplishing more challenging multimodal problems.

One core challenge in the path to achieving more general MLLMs is to develop better visual representations for diverse visual data. Visual data exhibit significant complexity and diversity, characterized by variations in collection sources, targeted visual tasks, specific contents, and resolution qualities. Existing approaches often simply treat all kinds of visual inputs uniformly, overlooking the variations in visual content and the specific demands of different applications. For example, early MLLMs (Alayrac et al., 2022; Li et al., 2023; Bai et al., 2023) attempt to standardize these diverse visual inputs by converting them into a fixed resolution so that pre-trained CLIP encoders can be used to extract high-quality visual representations that are well aligned with language contents. Recent advancements in MLLMs (Liu et al., 2024c; Xu et al., 2024b; Yao et al., 2024) extend the idea by introducing dynamic partitioning (Liu et al., 2024c) as a means to produce high-resolution visual representations while utilizing the strong CLIP models for encoding. However, the solution remains a compromise due to the lack of high-quality multi-modal encoders that support native resolution inputs. Supporting native resolution in an on-demand manner for visual inputs emerges as a more generalized and effective solution for visual understanding in MLLMs, offering several advantages: it prevents information loss by utilizing the entire image as input, thereby resolving extreme corner cases, and it

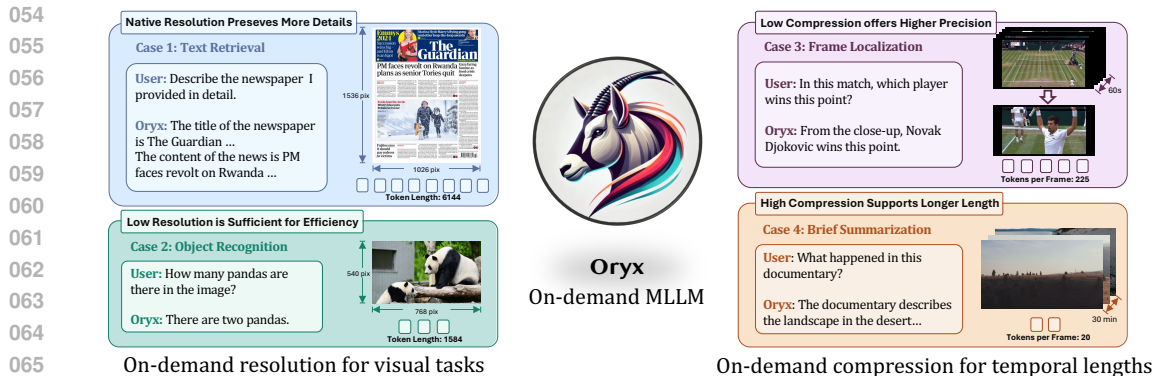


Figure 1: **Our main idea of on-demand multimodal understanding.** Different visual data and tasks may require different input resolutions and compression ratios on visual tokens. Supporting arbitrary resolution in an on-demand manner for visual inputs emerges as a more general and effective solution for visual understanding in MLLMs.

enhances efficiency and naturalness, resulting in better overall performance. As illustrated in Figure 1, optimizing for resolution and compression can lead to greater efficiency and meet practical needs: high resolution is crucial for text-relevant tasks, while object-level tasks may require only simple images, some applications may need to summarize extremely long videos while others maintain high precision for each frame.

In this paper, we explore on-demand MLLMs for comprehensive spatial-temporal understanding by introducing evolved architectural designs and propose the new Oryx model, which aims to address these challenges and enhance the functionality of MLLMs. Oryx is a unified spatial-temporal understanding MLLM framework that adeptly handles arbitrary visual resolutions, varying temporal lengths, and a diverse range of tasks in an on-demand manner. Oryx is characterized by the following key contribution: 1) A pre-trained visual encoder OryxViT is developed to generate LLM-friendly visual representations at native resolutions. Equipped with adaptive positional embeddings and variable-length self-attention, OryxViT can efficiently process visual data with different sizes in parallel; 2) Dynamic compression technique that adjusts downsampling ratios arbitrarily while fusing the information through a shared projector, thereby supporting a seamless switch between 1x to 16x compression. The new design enables Oryx to easily process extremely long inputs with up to 16x compression while maintaining high recognition precision for inputs that do not require compression; 3) Enhanced data curation and training strategies that help Oryx achieve pioneering performance in multimodal images, videos, and 3D data understanding and easily adapt to arbitrary input resolution and tasks simultaneously.

We evaluate the Oryx model on a wide range of multi-modal benchmarks, demonstrating remarkable performance in both spatial and temporal understanding across image, video, and multi-view 3D data. Notably, the Oryx model excels in general and long-form video comprehension, achieving competitive results with a 7B model size and surpassing models up to 72B in size with our 34B variant. This has led to new state-of-the-art results among open-source models on several benchmarks, including NextQA (Xiao et al., 2021), Perception Test (Ptraucean et al., 2024), MMBench-Video (Fang et al., 2024), and MVBench (Li et al., 2024c) for general video understanding and MLVU (Zhou et al., 2024), LongVideoBench (Wu et al., 2024) for long-form video benchmark. Additionally, the Oryx model shows strong performance in 2D and 3D spatial understanding, outperforming mainstream image-based MLLMs and 3D-specific LLMs, respectively, benefiting from its unified training strategy.

2 RELATED WORK

Visual Encoding in Multi-Modal LLMs. Multi-modal LLMs depend on visual encoders to extract visual features and employ connectors for aligning visual features with the LLMs. Alayrac et al. (2022) and Li et al. (2023) utilize attention to capture visual features and align the visual encoder

with LLMs through learnable queries, which may struggle when not adequately trained. LLaVA (Liu et al., 2024d;b;f) utilizes a simple MLP to connect the visual encoder with LLMs, while Ranzinger et al. (2024) combines visual features from different encoders for enhancement. However, they are limited to fixed resolutions, which may hinder their ability to capture detailed information and restrict their flexibility in understanding images with varying aspect ratios. Recent advancements in high-resolution perception (Liu et al., 2024c; Xu et al., 2024b; Yao et al., 2024) have primarily been driven by dynamic partitioning, which divides an image into multiple patches of equal resolution. While this method can manage high-resolution images, it is inefficient, and the partitioning process may result in the loss of critical information present in the original image. In this paper, we introduce OryxViT, an innovative step in visual encoding that enables native resolution perception.

Multi-modal LLMs Supporting Diverse Contexts and Tasks. Recent advancements in MLLMs have enabled them to comprehend a wide range of complex visual inputs from different tasks with various contexts. Lin et al. (2023a); Cheng et al. (2024); Qian et al. (2024) try to combine image and video perception, and Zhang et al. (2024a) focuses on long-form video analysis with extended context lengths. 3D-LLM (Hong et al., 2023) made the first attempt to enable MLLMs to comprehend 3D environments. Li et al. (2024b); Jiang et al. (2024) investigate interleaved data training to handle multi-image scenarios, and Li et al. (2024a) unifies single-image, multi-image, and video settings through improved data curation and training strategies. While previous approaches relied heavily on enhanced data curation to achieve multi-task comprehension, we propose a novel framework that represents complex visual inputs with cohesive representations. Our model is capable of processing visual contexts of arbitrary sizes, videos of varying lengths, and 3D data seamlessly, supporting various context lengths and versatile tasks.

3 METHODS

In this section, we provide a detailed explanation of Oryx’s contribution. Our design is segmented into two primary components: [the architecture and the data curation & training pipeline](#), which are elaborated upon in Section 3.1 and 3.2, respectively. We describe our innovative architecture to process native and on-demand visual inputs within MLLMs, as illustrated in Figure 2, enabling the development of a model capable of generalizing across image, video, and 3D data. Furthermore, we outline the simple yet effective training pipeline of the Oryx model.

3.1 ORYX ARCHITECTURE: MLLM WITH NATIVE AND FLEXIBLE VISUAL INPUTS

3.1.1 VISUAL REPRESENTATIONS WITH NATIVE RESOLUTION

Resizing and regularizing visual inputs, including images and videos, is a necessary and effective preprocessing step. Common practice typically involves resizing and cropping visual inputs to a fixed resolution with a square shape. However, such processes may negatively impact the performance of vision backbones, as previous studies on vision recognition have demonstrated the effectiveness of maintaining visual content in its original form. NaViT (Dehghani et al., 2024) leverages the characteristics of the vanilla ViT (Dosovitskiy, 2020), introducing a pack sequence operation that accommodates images of any aspect ratio and resolution for efficient training. Similarly, Flex-iViT (Beyer et al., 2023) and ViTAR (Fan et al., 2024) incorporate randomly resized images during training to develop a Vision Transformer capable of handling inputs of varying resolutions.

Despite these advancements, the effectiveness of native or arbitrary resolution in the realm of MLLM has barely been explored. Most existing MLLMs integrate original image-text visual encoders such as CLIP (Radford et al., 2021) and SigLIP (Zhai et al., 2023) to encode input visual data. We posit that MLLMs provide an optimal environment for processing visual representations at their native resolution for two primary reasons: (1) the sources and tasks associated with visual inputs are diverse, necessitating varying demands and formats; (2) the token lengths in MLLMs are inherently dynamic, particularly in the language component. Consequently, the dynamic representation of visual context aligns seamlessly with subsequent processing stages.

In Vision Transformer (ViT) models (we omit the class token here for simplification), given the visual input $\{x\} \in H \times W$, where typically $H \neq W$, the ViT first resizes the visual input into $\{x\} \in N \times N$. The resized image is then passed through patch embedding layers, which partition the image into

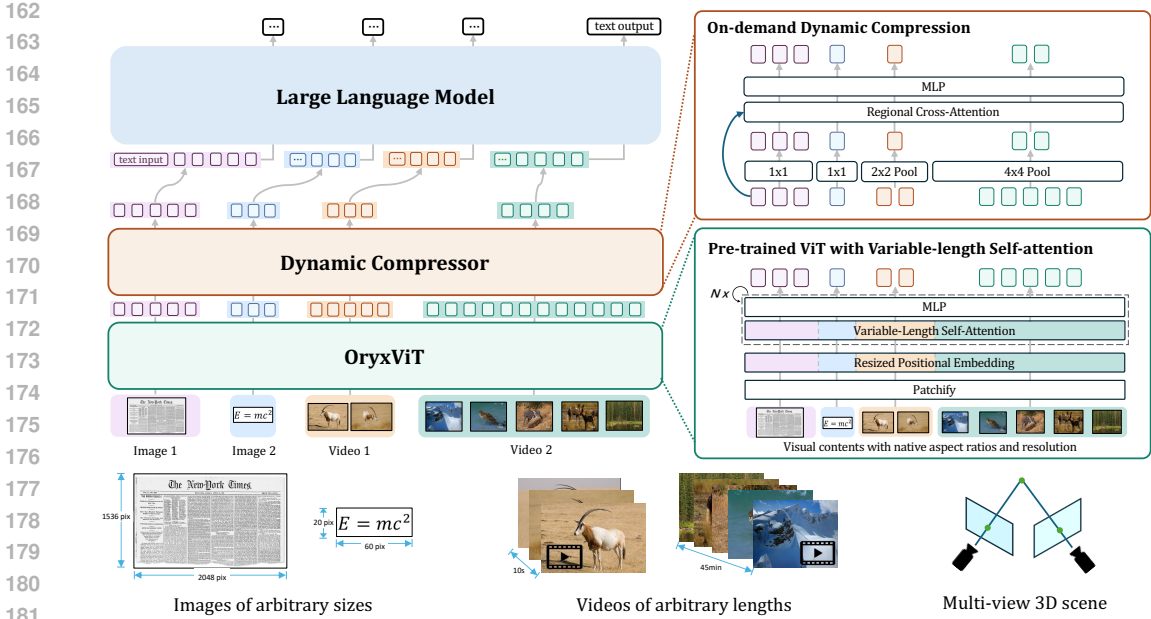


Figure 2: **Overview of Oryx architecture.** Oryx offers two options to process visual inputs with arbitrary spatial sizes and temporal lengths in an on-demand manner. 1) A pre-trained OryxViT equipped with variable-length self-attention to encode visual features with native aspect ratios and resolution. 2) A dynamic compressor offering on-demand compression on visual tokens while maintaining a unified token form.

patches of size $p \times p$, resulting in a sequence of patches $\{x\} \in (N/p) \times (N/p)$. Conventional Vision Transformers utilize a fixed-size position embedding matrix P corresponding to the predefined image size $N \times N$. However, when processing visual inputs at their native resolution $\{x\} \in [H/p] \times [W/p]$, directly resizing P to $[H/p] \times [W/p]$ can lead to a significant drop in accuracy, as demonstrated in previous works (Dehghani et al., 2024; Beyer et al., 2023).

To address the issue of native resolution processing, we introduce a visual encoder named OryxViT, which builds upon the advanced SigLIP (Zhai et al., 2023) models and is based on the Vision Transformer (Dosovitskiy, 2020) architecture. We modify the vision encoder by incorporating a sufficiently large position embedding matrix P that accommodates the maximum target input sizes (2048×2028 in our models, which can also be further interpolated for even larger inputs). For each visual input, we rescale the original position embeddings into $P \in [H/p] \times [W/p]$ using bilinear interpolation and apply the transformation $x = x + P$. The adaptation strategy for the newly defined P under native input resolution follows the training format of common MLLMs. We employ a relatively lightweight LLM as the language interface, keeping the vision encoder’s parameters unfrozen while freezing most of the other parameters. We collect training data pairs from multiple vision-language tasks including captioning, OCR, visual question answering, etc. **The pre-training strategy for the proposed visual encoder OryxViT under native input resolution follows the training format of common MLLMs. We employ a relatively lightweight LLM as the language interface, keeping the vision encoder’s parameters unfrozen while freezing most of the other parameters. Details for the training settings and datasets can be referred to in the Appendix.**

A significant challenge is managing the dynamic sequence length $N = [H/p] \times [W/p]$ for the Vision Transformer during batch processing, where we propose the Variable-Length Self-Attention strategy to address this issue. For visual patches with lengths N_1, N_2, \dots, N_b in a batch of size b , we concatenate the patches across the sequence dimensions into a shape of $[1, \sum_{i=1}^b N_i, C]$ before feeding them into the transformer blocks. We utilize the variable-length attention operator provided in flash attention (Dao et al., 2022) to compute the attention for each visual input within the batch independently. With these designs, our OryxViT can efficiently process visual signals of varying aspect ratios in batch mode, maintaining a forward speed comparable to that of conventional fixed-resolution visual encoders. **We also provide the detailed speed test for OryxViT in the Appendix to demonstrate the efficiency.**

3.1.2 ON-DEMAND DYNAMIC COMPRESSION SUPPORTING LONG VISUAL CONTEXT

With visual inputs varying in temporal length and resolution, such as some video data lasting tens of minutes, treating all inputs equally, as in most previous works (Zhang et al., 2024a; Xue et al., 2024), leads to inefficient computational costs. To address this, we propose a Dynamic Compressor, which is capable of performing higher compression ratios for longer contexts. Our design unifies visual contexts with different compression ratios into a consistent pattern, allowing us to control the overall visual sequence length on demand.

Using the visual representation feature map f , the compression serves as the bridge between vision and language modalities. We implement downsample layers with varying ratios to accommodate different input lengths. Specifically, we categorize the visual context into pure images, short videos, and long videos, applying downsample layers d_1, d_2, d_3 respectively. In our implementation, we set $d_3 = 4d_2 = 16d_1$, therefore the token length of frames in the long videos is reduced to $\frac{1}{16}$ of that of images with the same resolution. **We satisfy the downsampling ratio $r_1 < r_2 < r_3$ for layer d_1, d_2, d_3 to reduce the token length for frames in videos.**

We obtain the low-resolution feature map $f_L = d_i(f_H), i = 1, 2, 3$ from the high-resolution feature map f_H . To mitigate the effects of downsampling, we employ an attention operation to facilitate interaction between f_L and f_H . Specifically, for a downsample ratio r , we treat $f_L \in \mathbb{R}^{N \times C}$ as the query tensor \mathbf{Q} and $f_H \in \mathbb{R}^{N \times r^2 \times C}$ as the key tensor \mathbf{K} and value tensor \mathbf{V} . Each patch in the low-resolution f_L interacts with r^2 neighboring patches in the high-resolution f_H through a cross-attention operation, formulated as follows:

$$f_L = f_L + \text{Softmax}\left(\frac{\phi_q(\mathbf{Q})\phi_k(\mathbf{K}^T)}{\sqrt{d_k}}\right)\mathbf{V} \quad (1)$$

where we define the query and key projection layers, denoted as ϕ_q and ϕ_k , to project the query and key tensors into lower dimensions. To maintain the original features from the visual encoder and limit the number of linear projection layers, we omit the value and output projection layers commonly used in attention modules. Then we utilize a shared MLP across multiple downsample modules to project the compressed low-resolution features into the embedding space of the language model. We preserve the interactions between different downsample ratios through the shared projection. Upon completion of the dynamic compression module, the final visual representation features are flattened and integrated into the sequence of visual tokens among the text tokens. This combined sequence is then fed into the language model for token prediction.

3.2 DATA CURATION & TRAINING PIPELINE

3.2.1 ONE MODEL FOR ALL: IMAGE, VIDEO, AND 3D UNDERSTANDING

Previous work (Li et al., 2024a; Chen et al., 2024b; QwenTeam, 2024b) has demonstrated the coexistence of MLLMs that support both image and video modalities. Building on this foundation, our research aims to extend the capabilities of these models to handle more diverse contexts, varying lengths of content, and a broader range of tasks. To achieve this, we meticulously curate a training dataset specifically designed for extremely long-form videos. Additionally, we further incorporate spatial-relevant knowledge through coarse correspondence markers among multi-frame visual inputs to make Oryx 3D-aware.

Long-Form Temporal Training with Needle-In-A-Haystack. The key ability for processing long-form video inputs is the identification of specific information within an extensive context, akin to the "needle-in-a-haystack" task in the NLP field. To enhance the Oryx model’s capability to pinpoint details, we prepare long-form temporal needle-in-a-haystack training data. Specifically, we source video samples from the MovieNet (Huang et al., 2020) dataset, which comprises an average of 1000 frames per movie and an average duration of 45 minutes, thereby providing a natural setting for retrieving designated targets. We devise two tasks to train the model: captioning and differing. The captioning task requires the model to generate captions for frames at specific indices, while the differing task involves identifying differences between two frames given their indices. The training corpus is generated using **SOTA LLMs** GPT-4o, which produces captions for single frames or frame pairs. These captioned frames are then reinserted into the overall movie sequences, ensuring the training data maintains contextual integrity.

Learning Spatial-Aware Knowledge via Coarse Correspondences. Recent advancements have focused on enhancing multi-modal LLMs with 3D understanding capabilities. These approaches primarily treat 3D tasks as multi-image inputs. However, unlike video inputs, multi-view images generated from 3D environments lack temporal or trajectory cues, which are essential for MLLMs to accurately process sequential data. As a result, previous methods often struggle to achieve correct spatial understanding when evaluated against 3D benchmarks.

Building on the work of (Liu et al., 2024a), we introduce coarse correspondences into our training dataset. The core concept is to assign a consistent label to the same object across different frames, allowing the model to better capture spatial correlations across multiple views. This approach aims to enhance the model’s ability to develop a more accurate 3D spatial understanding. Specifically, we utilize Track-Anything (Yang et al., 2023b) as our tracking model to generate coarse correspondences for the ScanQA training set. These data are then incorporated into the final training set.

3.2.2 TRAINING PIPELINE

The training pipeline of Oryx is lightweight and direct in a 2-stage strategy. We start from a well-trained vision tower OryxViT and a Large Language Model. The first stage involves only image data following common practice (Liu et al., 2024d;b). The second stage uses a mixture of data from images, videos, and corresponding 3D frames and we train the multi-source data jointly thanks to our unified design. All of our training data are collected from open-source datasets, therefore ensuring the reproducibility of the Oryx model and holding room for improvement with better data curation.

Stage 1: Text-Image Pre-training and Supervised Fine-tuning. In the first stage of our training process, we focus on developing the foundational vision-language capabilities of the Oryx model using image data. This stage begins with a pre-training phase to train the dynamic compressor component [with the basic image captioning data](#) a dataset of 558k images in LLaVA-1.5 (Liu et al., 2024b). Following this, we gather a collection of 4 million supervised fine-tuning image-text pairs that focus on high-quality knowledge learning. This data is sourced from various open-source academic datasets, including LLaVA-NeXT (Liu et al., 2024c), Cauldron (Laurençon et al., 2024), and Cambrian-1 (Tong et al., 2024). It is important to note that we do not incorporate large-scale pre-training stages as described in (Li et al., 2024a) or employ exclusive supervised fine-tuning data such as those in (Lin et al., 2023b; Bai et al., 2023), as our primary objective is to validate the effectiveness of our unified Oryx architecture.

Stage 2: Joint Supervised Fine-tuning. In Stage 2, we further conduct a supervised fine-tuning procedure following the initial stage, aiming to jointly train the Oryx model with image, video, and 3D-aware visual inputs. The image training data is sampled from the dataset collected during the supervised fine-tuning phase of Stage 1, ensuring a balanced ratio of image and video data by utilizing around 600k image-text pairs. For video data, we source both comprehensive and multiple-choice datasets from open-source video repositories. Comprehensive datasets, which include question-answering and captioning tasks, are integrated using VideoChatGPT-Plus (Maaz et al., 2024), ShareGPT4Video (Chen et al., 2024a) and LLaVA-Hound (Zhang et al., 2024b). To enhance performance on multiple-choice benchmarks, we further incorporated Cinepile (Rawal et al., 2024), NextQA (Xiao et al., 2021) and PerceptionTest (Patraucean et al., 2024) into our training dataset. Additionally, we include video samples of needle-in-a-haystack data generated by GPT-4o (OpenAI, 2024) for long-form video learning and spatial-aware 3D multi-frame samples from the ScanQA (Azuma et al., 2022) training dataset, culminating in a total of around 650k video samples. The supervised fine-tuning strategy in this stage mirrored that of Stage 1, ensuring consistency in the training approach.

4 EXPERIMENTS

We conduct comprehensive experiments across multiple vision-language benchmarks to demonstrate the effectiveness of our method. In this section, we present the main results on general video understanding benchmarks (Sec. 4.1), long-form video benchmarks (Sec. 4.2), 2D & 3D spatial understanding benchmarks (Sec. 4.3) and compare our method with other state-of-the-art video MLLMs. Finally, we provide analysis experiments and critical ablation studies on design elements.

Table 1: **General Temporal Understanding.** We conduct experiments on four multiple-choice benchmarks and three generation benchmarks comprehensively and report the main score for each dataset. Oryx exhibits superior performance under a wide range of open-sourced video MLLMs.

Model	Size	VideoMME	NextQA	MVBench	PercepTest	MMB-Video	VCG	VDC
<i>Proprietary Models</i>								
GPT-4V (OpenAI, 2023b)	-	59.9/63.3	-	43.7	-	1.53	4.06	4.00
GPT-4o (OpenAI, 2024)	-	71.9/77.2	-	-	-	1.63	-	-
Gemini-1.5-Pro (GeminiTeam, 2024)	-	75.0/81.3	-	-	-	1.30	-	-
<i>Open-Sourced Video MLLMs</i>								
VideoChat2-HD (Li et al., 2024c)	7B	45.3/55.7	79.5	62.3	47.3	1.18	3.10	-
VideoLLaMA2 (Cheng et al., 2024)	7B	47.9/50.3	-	54.6	51.4	-	3.13	-
LLaVA-OneVision (Li et al., 2024a)	7B	58.2/61.5	79.4	56.7	49.7	-	3.51	3.75
Kangaroo (Liu et al., 2024e)	8B	56.0/57.6	-	61.1	-	1.44	-	-
VideoCCAM (Fei et al., 2024)	9B	53.9/56.1	-	64.6	-	-	-	-
LLaVA-Next-Video (Zhang et al., 2024c)	34B	52.0/54.9	70.2	-	51.6	-	3.34	3.48
PLLaVA (Xu et al., 2024a)	34B	-	-	58.1	-	-	-	-
VILA-1.5 (Lin et al., 2023b)	40B	60.1/61.1	67.9	-	54.0	-	3.36	3.37
VideoLLaMA2 (Cheng et al., 2024)	72B	61.4/63.1	-	62.0	57.5	-	3.16	-
LLaVA-OneVision (Li et al., 2024a)	72B	66.2/69.5	80.2	59.4	66.9	-	3.62	3.60
Oryx	7B	59.1/63.3	81.9	63.9	70.0	1.47	3.53	3.76
Oryx	34B	63.2/67.4	83.5	64.7	71.4	1.49	3.51	3.66

4.1 GENERAL TEMPORAL UNDERSTANDING

Setup. We present the experimental results on general multi-modal video understanding datasets, as video data provides comprehensive insights into visual-language abilities, especially when dealing with complex and diverse visual inputs. We select several representative and popular benchmarks, encompassing both multiple-choice and generation tasks for evaluation. We conduct evaluations on four multiple-choice benchmarks. VideoMME (Fu et al., 2024) performs a full spectrum of diverse videos and varying temporal lengths. NextQA (Xiao et al., 2021) is a classic benchmark for video reasoning. MVBench (Li et al., 2024c) performs 20 challenging video tasks for video comprehension. Perception Test (Patraucean et al., 2024) focuses on the perception and reasoning skills of MLLMs. For generation-relevant benchmarks scored by advanced proprietary models, we integrate evaluations on MMBench-Video (Fang et al., 2024), Video-ChatGPT(VCG) (Maaz et al., 2023), and Video Detailed Caption(VDC) benchmarks. Following common practice, GPT-4-1106 (OpenAI, 2023c) is used as the evaluator for MMBench-Video (Fang et al., 2024), GPT-3.5-0613 (OpenAI, 2023a) is employed for Video-ChatGPT (Maaz et al., 2023) and Video Detailed Caption.

Results. The experimental results, as detailed in Table 1, demonstrate that the Oryx model achieves highly competitive outcomes in general video understanding tasks. We surpass a broad spectrum of near-term video-specific MLLMs and establish new state-of-the-art. The Oryx model attains tier-1 performance among small-sized MLLMs (approximately 7B parameters) and exhibits competitive performance when compared to larger MLLMs (exceeding 30B parameters), even rivaling models with 72B parameters. On the VideoMME benchmark (Fu et al., 2024) with subtitles, the Oryx models achieve mean accuracies of 62.6 and 67.4. Oryx also demonstrates robust performance across various multiple-choice datasets by surpassing previous state-of-the-art results by 3.3% and 4.5% on NextQA (Xiao et al., 2021) and Perception Test (Patraucean et al., 2024). Additionally, the Oryx model performs convincingly on GPT-eval benchmarks, with an average score of 1.49 on MMBench-Video (Fang et al., 2024), 3.53 and 3.76 on VideoChatGPT (Maaz et al., 2023) and Video Detailed Caption, respectively. Remarkably, the Oryx model outperforms advanced proprietary models such as GPT-4V (OpenAI, 2023b) and Gemini-1.5-Pro (GeminiTeam, 2024) on several of the most challenging benchmarks.

4.2 LONG-FORM TEMPORAL UNDERSTANDING

To further demonstrate the exceptional long-context understanding capability of our method, we conduct experiments on benchmarks specifically designed for long video evaluation. Additionally, we employ the video needle-in-a-haystack task to illustrate our model’s ability to handle extremely lengthy video content in Appendix C.1.

Table 2: **Long-Form Temporal Understanding.** We show results on three mainstream long-form temporal understanding datasets, each featuring video inputs of tens of minutes in duration. Oryx demonstrates superior performance, achieving state-of-the-art results and surpassing several proprietary models across various benchmarks.

Model	Size	MLVU	LongVideoBench	VideoMME-Long	
				w/o subs	w subs
<i>Proprietary Models</i>					
GPT-4V (OpenAI, 2023b)	-	49.2	60.7	53.5	56.9
GPT-4o (OpenAI, 2024)	-	64.6	66.7	65.3	72.1
Gemini-1.5-Pro (GeminiTeam, 2024)	-	-	64.4	67.4	77.4
<i>Open-Sourced Video MLLMs</i>					
VideoLLaMA2 (Cheng et al., 2024)	7B	48.5	-	42.1	43.8
LongVA (Zhang et al., 2024a)	7B	56.3	-	46.2	47.6
LLaVA-OneVision (Li et al., 2024a)	7B	64.7	-	-	-
Kangaroo (Liu et al., 2024e)	8B	61.0	54.8	46.6	49.3
LongVILA (Xue et al., 2024)	8B	-	-	39.7	-
VideoCCAM (Fei et al., 2024)	14B	63.1	-	46.7	49.9
LLaVA-Next-Video (Zhang et al., 2024c)	34B	-	50.5	-	-
PLLaVA (Xu et al., 2024a)	34B	-	53.2	-	-
VILA-1.5 (Lin et al., 2023b)	40B	56.7	-	53.8	55.7
LLaVA-OneVision (Li et al., 2024a)	72B	66.4	61.3	60.0	62.4
Oryx	7B	67.5	56.3	51.3	56.8
Oryx	34B	70.8	62.2	53.9	58.0

Setup. We select three mainstream and representative benchmarks specifically designed for long video understanding, ensuring a comprehensive evaluation of long video inputs. MLVU (Zhou et al., 2024), encompasses videos ranging from 3 minutes to 2 hours and includes 9 distinct tasks that assess both global and local information within the video content. LongVideoBench (Wu et al., 2024) presents a primary challenge of retrieving and reasoning over a dataset comprising 3k long video inputs. Additionally, we utilize the long video subset of the VideoMME (Fu et al., 2024) benchmark, which features videos with lengths ranging from 30 minutes to 60 minutes.

Results. Results are shown in Table 2, which highlights the efficacy of our unified and on-demand design across varying temporal lengths and our further efforts in the context of long video retrieval. The Oryx model exhibits a remarkable capability in understanding long-form video content. Specifically, our Oryx-7B model surpasses all existing 7B model series on long video benchmarks. Furthermore, the Oryx-34B model showcases strong performance across larger MLLMs, achieving a mean accuracy improvement of 4.4% and 0.9% over previous state-of-the-art models equipped with 72B parameter LLMs on the MLVU (Zhou et al., 2024) and LongVideoBench (Wu et al., 2024) benchmarks, respectively. Notably, the Oryx-34B model also outperforms GPT-4o (OpenAI, 2024) on the challenging MLVU (Zhou et al., 2024) benchmark by a margin of 6.2%, underscoring its advanced capabilities in long video understanding.

4.3 2D & 3D SPATIAL UNDERSTANDING

As we perform a general solution across spatial and temporal understanding, we incorporate image and 3D benchmarks to thoroughly evaluate our model, which shows the foundation multi-modal capabilities of Oryx and the potential for extending to more visual tasks, formats, and circumstances.

Image Benchmarks. We select a diverse set of mainstream and representative image benchmarks to evaluate the model’s proficiency in image understanding. Specifically, we included MMBench (Liu et al., 2023a) and MMMU (Yue et al., 2024) to assess general image understanding capabilities, and DocVQA (Mathew et al., 2021), OCRBench (Liu et al., 2023b), AI2D (Kembhavi et al., 2016), and TextVQA (Singh et al., 2019) to evaluate the model’s performance on specific tasks such as document recognition, OCR, text understanding tasks, etc. The results are summarized in Table 3. Notably, the Oryx model maintains pioneering results on image benchmarks, such as an 84.5% mean accuracy on MMBench (Liu et al., 2023a) and a 91.4% accuracy on DocVQA (Mathew et al., 2021). Such results demonstrate the effectiveness of our method in comprehending images with more simple and lightweight training pipelines, data curation, and strategies compared with concurrent works.

Table 3: **Image Understanding.** We conduct 2D spatial understanding tasks on six representative image benchmarks, including general and task-specific benchmarks. Our Oryx model achieves tier-1 performance across a wide range of MLLMs.

Model	Size	MMBench	MMMUs	DocVQA	OCRBench	AI2D	TextVQA
Deepseek-VL (Lu et al., 2024)	7B	73.2	36.6	-	456	-	64.7
Monkey (Li et al., 2024d)	7B	72.4	40.7	-	534	68.5	-
LLaVA-NeXT (Liu et al., 2024c)	8B	72.1	41.7	78.2	531	71.6	-
Bunny-LLama3 (He et al., 2024)	8B	77.2	43.3	-	444	69.4	-
Cambrian-1 (Tong et al., 2024)	8B	75.9	42.7	77.8	624	73.6	71.7
VILA-1.5 (Lin et al., 2023b)	8B	75.3	38.6	-	-	-	68.5
Idefics2 (Laurençon et al., 2024)	8B	76.7	43.0	-	-	-	73.0
Yi-VL (Young et al., 2024)	34B	-	45.1	-	290	65.9	-
LLaVA-NeXT (Liu et al., 2024c)	34B	79.3	49.7	84.0	574	74.9	-
Cambrian-1 (Tong et al., 2024)	34B	81.4	49.7	75.5	600	79.7	76.7
VILA-1.5 (Lin et al., 2023b)	40B	82.4	51.9	-	-	-	73.4
Oryx	7B	81.4	47.1	90.1	713	79.7	75.7
Oryx	34B	84.5	50.3	91.4	743	81.0	77.8

Table 4: **3D Spatial Understanding.** We use the popular ScanQA (Azuma et al., 2022) dataset and evaluate the relevant scores. We compare the Oryx model with 3D-specific models together with general open-source MLLMs. Oryx excels in 3D spatial understanding tasks, highlighting its versatility across various applications.

Model	Size	METEOR	ROUGE-L	CIDEr	BLEU-1	BLEU-2
<i>3D-Specific Models</i>						
VoteNet+MCAN (Qi et al., 2019)	-	11.4	29.8	54.7	28.0	16.7
ScanQA (Azuma et al., 2022)	-	11.5	30	55.4	26.9	16.6
ScanRefer+MCAN (Chen et al., 2020)	-	13.1	33.3	64.9	30.2	20.4
3D-LLM (Hong et al., 2023)	-	14.5	35.7	69.4	39.3	25.2
<i>General Open-Source MLLMs</i>						
BLIP2 (Li et al., 2023)	-	11.3	26.6	45.7	29.7	16.2
Flamingo (Alayrac et al., 2022)	7B	11.3	31.1	55	25.6	15.2
Mantis (Jiang et al., 2024)	7B	-	16.1	-	-	-
LLaVA-Next-Interleave (Li et al., 2024b)	14B	-	34.5	-	-	-
LLaVA-OneVision (Li et al., 2024a)	72B	-	35.8	-	-	-
Oryx	7B	14.5	35.5	69.1	35.8	24.4
Oryx	34B	15.0	37.3	72.3	39.6	26.7

3D Spatial Understanding. We conduct the 3D spatial understanding experiments on the classic ScanQA validation set, following the protocol established by previous work (Azuma et al., 2022; Hong et al., 2023; Liu et al., 2024a). We incorporate advanced baseline models, including 3D-specific models and general open-source MLLMs supporting 3D spatial tasks for a comprehensive comparison. As shown in Table 4, the Oryx model not only outperforms previous specialized models designed for 3D understanding, but also surpasses the recently updated general MLLMs and specially designed 3D-LLM (Hong et al., 2023). These results underscore the robust adaptability of our method in addressing 3D spatial tasks.

4.4 ANALYSIS

Effects of resolution and resize strategy across benchmarks. To illustrate the effectiveness of the advanced native representation for visual inputs, we conduct ablation analysis experiments on the effects of resolution across multi-modal benchmarks in Figure 3. We compare inputs with native resolution to inputs rescaled to specific overall number of pixels while maintaining the original aspect ratios. The left figure presents the scores on several benchmarks, where we utilize images scaled to 768^2 pixels, 1024^2 pixels, images with native resolution, and larger images (2x area) with native resolution. The results indicate that native resolution consistently outperforms fixed sizes, with the performance gap becoming more pronounced in the DocVQA and OCRBench datasets. These datasets require the visual encoder to process more natural image inputs for text understanding. Additionally, further enlarging the resolution does not yield significant gains in most benchmarks. The right figure illustrates the performance trends on MMBench and OCRBench with varying visual input resolutions. Our findings suggest that while larger images generally lead to better performance, maintaining the native resolution emerges as a simple yet effective strategy for optimizing performance.

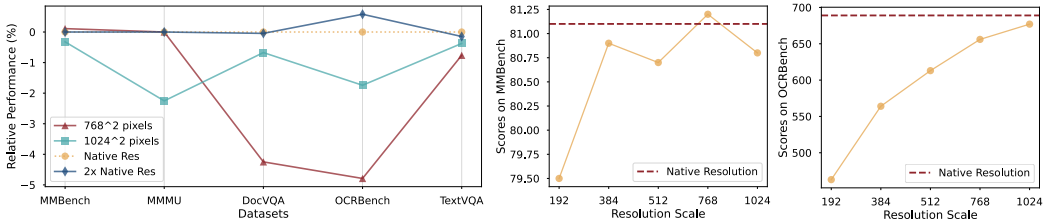


Figure 3: **Effects of resolution and resize strategy across benchmarks.** The left figure shows the performance across benchmarks with fixed size, native size, and larger images. The right figure shows the trend of performance with varying resolutions, where we illustrate the performance of native resolution for reference. The text-relative benchmarks show more sensitivity to the resolution scale, while all the benchmarks benefit from the visual inputs with native resolution.

Table 5: **Ablations on the Oryx Architecture.** We evaluate our design of two core architectures within the Oryx model. (a) examines the impact of the visual encoder and the method of processing visual inputs, demonstrating the superiority of native visual representations compared with dynamic partition and the strong visual-text alignment capability of OryxViT. (b) assesses the influence of dynamic compression modules in comparison to conventional MLP connectors, revealing significant performance gains due to improved fusion of image and video data. Various downsampling approaches were tested, with average pooling yielding the best performance.

(a) Ablation study on Visual Encoder.

Visual Enc.	Res.	DocVQA	OCRBench	MMBench
SigLIP	Partition	74.8	531	68.0
SigLIP	Native	17.1	67	15.8
OryxViT	Partition	76.3	549	68.9
OryxViT	Native	78.5	572	69.3
OryxViT	Optimal	79.2	572	69.9

(b) Ablation Study on Compression Module.

Connector	Downsample	VideoMME	MLVU
MLP	Avg Pool	54.6	57.5
Dy.Compressor	Avg Pool	55.4	59.3
Dy.Compressor	DWConv	55.0	58.9
Dy.Compressor	Conv-MLP	54.7	58.5

Effectiveness of the Oryx Architecture. We conduct more ablation experiments on the design of the Oryx architecture in Table 5. For the visual representation, we compare OryxViT with the mainstream SigLIP visual encoder. Our comparison highlights the superior alignment performance of OryxViT. Additionally, we fairly compare previous dynamic partition approaches with visual inputs of native resolutions. We conclude from the results that the previous mainstream multi-modal encoder SigLIP (Zhai et al., 2023) fails to process native visual input and only works on fixed resolution with the dynamic partition trick. On the contrary, the OryxViT benefits from the visual inputs at native resolution, which is superior to the partition approach. As an arbitrary visual encoder, we are also curious about the limit of resolutions, where we find that searching for the optimal anchor resolution leads to better performance (the last line in Table 5 (a)). However, for the sake of fairness and efficiency, we do not employ this optimization in our primary evaluations. We report our results on several representative image benchmarks, including DocVQA, OCRBench, and the general MMBench datasets, using a subset of image training data for efficient training.

For the connector module, we compare the proposed dynamic compressor with the popular and straightforward MLP architecture. The dynamic compressor demonstrates superior performance on both general and long temporal benchmarks by better fusing multi-modal data. Furthermore, our analysis reveals that average pooling yields better results for higher compression visual inputs compared to parameter-reliant approaches such as DWConv and Conv-MLP. This improvement is likely due to the parameter-free nature of average pooling, which preserves the distribution of visual features, and more complex downsampling layers may not be effectively trained through the current training pipeline. Our analysis of the connector module is conducted on a subset of video training data to maintain training efficiency.

5 CONCLUSION

In this paper, we have introduced the Oryx series, a novel approach designed to handle diverse visual inputs across varying tasks, temporal lengths, and resolutions in an on-demand manner. The Oryx model stands out as a unified multi-modal framework for spatial-temporal understanding, leveraging

the innovative design of OryxViT for native resolution processing, the Dynamic Compressor for efficient data compression, and a robust joint training strategy. Our extensive evaluations demonstrate that the Oryx model achieves outstanding performance across a wide array of image, video, and 3D mainstream benchmarks. We hope that our work offers a novel perspective on multi-modal learning and paves the way for the development of more general MLLMs in future research endeavors.

REFERENCES

- Jean-Baptiste Alayrac, Jeff Donahue, Pauline Luc, Antoine Miech, Iain Barr, Yana Hasson, Karel Lenc, Arthur Mensch, Katherine Millican, Malcolm Reynolds, et al. Flamingo: a visual language model for few-shot learning. *NeurIPS*, 35:23716–23736, 2022.
- Daichi Azuma, Taiki Miyanishi, Shuhei Kurita, and Motoaki Kawanabe. Scanqa: 3d question answering for spatial scene understanding. In *CVPR*, pp. 19129–19139, 2022.
- Jinze Bai, Shuai Bai, Shusheng Yang, Shijie Wang, Sinan Tan, Peng Wang, Junyang Lin, Chang Zhou, and Jingren Zhou. Qwen-vl: A versatile vision-language model for understanding, localization, text reading, and beyond. 2023.
- Lucas Beyer, Pavel Izmailov, Alexander Kolesnikov, Mathilde Caron, Simon Kornblith, Xiaohua Zhai, Matthias Minderer, Michael Tschannen, Ibrahim Alabdulmohsin, and Filip Pavetic. Flexivit: One model for all patch sizes. In *CVPR*, pp. 14496–14506, 2023.
- Dave Zhenyu Chen, Angel X Chang, and Matthias Nießner. Scanrefer: 3d object localization in rgb-d scans using natural language. In *European conference on computer vision*, pp. 202–221. Springer, 2020.
- Lin Chen, Xilin Wei, Jinsong Li, Xiaoyi Dong, Pan Zhang, Yuhang Zang, Zehui Chen, Haodong Duan, Bin Lin, Zhenyu Tang, et al. Sharegpt4video: Improving video understanding and generation with better captions. *arXiv preprint arXiv:2406.04325*, 2024a.
- Zhe Chen, Jiannan Wu, Wenhai Wang, Weijie Su, Guo Chen, Sen Xing, Muyan Zhong, Qinglong Zhang, Xizhou Zhu, Lewei Lu, et al. Internvl: Scaling up vision foundation models and aligning for generic visual-linguistic tasks. In *CVPR*, pp. 24185–24198, 2024b.
- Zesen Cheng, Sicong Leng, Hang Zhang, Yifei Xin, Xin Li, Guanzheng Chen, Yongxin Zhu, Wenqi Zhang, Ziyang Luo, Deli Zhao, et al. Videollama 2: Advancing spatial-temporal modeling and audio understanding in video-llms. *arXiv preprint arXiv:2406.07476*, 2024.
- Tri Dao, Dan Fu, Stefano Ermon, Atri Rudra, and Christopher Ré. Flashattention: Fast and memory-efficient exact attention with io-awareness. *NeurIPS*, 35:16344–16359, 2022.
- Mostafa Dehghani, Basil Mustafa, Josip Djolonga, Jonathan Heek, Matthias Minderer, Mathilde Caron, Andreas Steiner, Joan Puigcerver, Robert Geirhos, Ibrahim M Alabdulmohsin, et al. Patch n’pack: Navit, a vision transformer for any aspect ratio and resolution. *NeurIPS*, 36, 2024.
- Alexey Dosovitskiy. An image is worth 16x16 words: Transformers for image recognition at scale. *arXiv preprint arXiv:2010.11929*, 2020.
- Qihang Fan, Quanzeng You, Xiaotian Han, Yongfei Liu, Yunzhe Tao, Huaibo Huang, Ran He, and Hongxia Yang. Vitar: Vision transformer with any resolution. *arXiv preprint arXiv:2403.18361*, 2024.
- Xinyu Fang, Kangrui Mao, Haodong Duan, Xiangyu Zhao, Yining Li, Dahua Lin, and Kai Chen. Mmbench-video: A long-form multi-shot benchmark for holistic video understanding. *arXiv preprint arXiv:2406.14515*, 2024.
- Jiajun Fei, Dian Li, Zhidong Deng, Zekun Wang, Gang Liu, and Hui Wang. Video-ccam: Enhancing video-language understanding with causal cross-attention masks for short and long videos. *arXiv preprint arXiv:2408.14023*, 2024.
- Chaoyou Fu, Yuhan Dai, Yondong Luo, Lei Li, Shuhuai Ren, Renrui Zhang, Zihan Wang, Chenyu Zhou, Yunhang Shen, Mengdan Zhang, et al. Video-mme: The first-ever comprehensive evaluation benchmark of multi-modal llms in video analysis. *arXiv preprint arXiv:2405.21075*, 2024.

- 594 GeminiTeam. Gemini 1.5: Unlocking multimodal understanding across millions of tokens of context.
595 *arXiv preprint arXiv:2403.05530*, 2024.
596
- 597 Muyang He, Yexin Liu, Boya Wu, Jianhao Yuan, Yueze Wang, Tiejun Huang, and Bo Zhao. Efficient
598 multimodal learning from data-centric perspective. *arXiv preprint arXiv:2402.11530*, 2024.
599
- 600 Yining Hong, Haoyu Zhen, Peihao Chen, Shuhong Zheng, Yilun Du, Zhenfang Chen, and Chuang
601 Gan. 3d-llm: Injecting the 3d world into large language models. *NeurIPS*, 36:20482–20494, 2023.
602
- 603 Qingqiu Huang, Yu Xiong, Anyi Rao, Jiase Wang, and Dahua Lin. Movienet: A holistic dataset for
604 movie understanding. In *ECCV*, pp. 709–727. Springer, 2020.
605
- 606 Dongfu Jiang, Xuan He, Huaye Zeng, Cong Wei, Max Ku, Qian Liu, and Wenhui Chen. Mantis:
607 Interleaved multi-image instruction tuning. *arXiv preprint arXiv:2405.01483*, 2024.
608
- 609 Aniruddha Kembhavi, Mike Salvato, Eric Kolve, Minjoon Seo, Hannaneh Hajishirzi, and Ali Farhadi.
610 A diagram is worth a dozen images. In *ECCV*, pp. 235–251. Springer, 2016.
611
- 612 Hugo Laurençon, Léo Tronchon, Matthieu Cord, and Victor Sanh. What matters when building
613 vision-language models? *arXiv preprint arXiv:2405.02246*, 2024.
614
- 615 Bo Li, Yuanhan Zhang, Dong Guo, Renrui Zhang, Feng Li, Hao Zhang, Kaichen Zhang, Yanwei
616 Li, Ziwei Liu, and Chunyuan Li. Llava-onevision: Easy visual task transfer. *arXiv preprint*
617 *arXiv:2408.03326*, 2024a.
- 618 Feng Li, Renrui Zhang, Hao Zhang, Yuanhan Zhang, Bo Li, Wei Li, Zejun Ma, and Chunyuan Li.
619 Llava-next-interleave: Tackling multi-image, video, and 3d in large multimodal models. *arXiv*
620 *preprint arXiv:2407.07895*, 2024b.
621
- 622 Junnan Li, Dongxu Li, Silvio Savarese, and Steven Hoi. Blip-2: Bootstrapping language-image
623 pre-training with frozen image encoders and large language models. In *ICML*, pp. 19730–19742.
624 PMLR, 2023.
- 625 Kunchang Li, Yali Wang, Yinan He, Yizhuo Li, Yi Wang, Yi Liu, Zun Wang, Jilan Xu, Guo Chen,
626 Ping Luo, et al. Mvbench: A comprehensive multi-modal video understanding benchmark. In
627 *CVPR*, pp. 22195–22206, 2024c.
628
- 629 Zhang Li, Biao Yang, Qiang Liu, Zhiyin Ma, Shuo Zhang, Jingxu Yang, Yabo Sun, Yuliang Liu, and
630 Xiang Bai. Monkey: Image resolution and text label are important things for large multi-modal
631 models. In *proceedings of the IEEE/CVF conference on computer vision and pattern recognition*,
632 2024d.
- 633 Bin Lin, Bin Zhu, Yang Ye, Munan Ning, Peng Jin, and Li Yuan. Video-llava: Learning united visual
634 representation by alignment before projection. *arXiv preprint arXiv:2311.10122*, 2023a.
635
- 636 Ji Lin, Hongxu Yin, Wei Ping, Yao Lu, Pavlo Molchanov, Andrew Tao, Huizi Mao, Jan Kautz,
637 Mohammad Shoeybi, and Song Han. Vila: On pre-training for visual language models, 2023b.
- 638 Benlin Liu, Yuhao Dong, Yiqin Wang, Yongming Rao, Yansong Tang, Wei-Chiu Ma, and Ranjay
639 Krishna. Coarse correspondence elicit 3d spacetime understanding in multimodal language model.
640 *arXiv preprint arXiv:2408.00754*, 2024a.
641
- 642 Haotian Liu, Chunyuan Li, Yuheng Li, and Yong Jae Lee. Improved baselines with visual instruction
643 tuning. In *CVPR*, pp. 26296–26306, 2024b.
- 644 Haotian Liu, Chunyuan Li, Yuheng Li, Bo Li, Yuanhan Zhang, Sheng Shen, and Yong Jae Lee.
645 Llava-next: Improved reasoning, ocr, and world knowledge, 2024c.
646
- 647 Haotian Liu, Chunyuan Li, Qingyang Wu, and Yong Jae Lee. Visual instruction tuning. *NeurIPS*, 36,
2024d.

- 648 Jiajun Liu, Yibing Wang, Hanghang Ma, Xiaoping Wu, Xiaoqi Ma, Xiaoming Wei, Jianbin Jiao,
649 Enhua Wu, and Jie Hu. Kangaroo: A powerful video-language model supporting long-context
650 video input. *arXiv preprint arXiv:2408.15542*, 2024e.
- 651 Yuan Liu, Haodong Duan, Yuanhan Zhang, Bo Li, Songyang Zhang, Wangbo Zhao, Yike Yuan, Jiaqi
652 Wang, Conghui He, Ziwei Liu, et al. Mmbench: Is your multi-modal model an all-around player?
653 *arXiv preprint arXiv:2307.06281*, 2023a.
- 654 Yuliang Liu, Zhang Li, Biao Yang, Chunyuan Li, Xucheng Yin, Cheng-lin Liu, Lianwen Jin,
655 and Xiang Bai. On the hidden mystery of ocr in large multimodal models. *arXiv preprint*
656 *arXiv:2305.07895*, 2023b.
- 657 Zuyan Liu, Yuhao Dong, Yongming Rao, Jie Zhou, and Jiwen Lu. Chain-of-spot: Interactive
658 reasoning improves large vision-language models. *arXiv preprint arXiv:2403.12966*, 2024f.
- 659 Zuyan Liu, Benlin Liu, Jiahui Wang, Yuhao Dong, Guangyi Chen, Yongming Rao, Ranjay Krishna,
660 and Jiwen Lu. Efficient inference of vision instruction-following models with elastic cache. *arXiv*
661 *preprint arXiv:2407.18121*, 2024g.
- 662 Haoyu Lu, Wen Liu, Bo Zhang, Bingxuan Wang, Kai Dong, Bo Liu, Jingxiang Sun, Tongzheng Ren,
663 Zhuoshu Li, Yaofeng Sun, et al. Deepseek-vl: towards real-world vision-language understanding.
664 *arXiv preprint arXiv:2403.05525*, 2024.
- 665 Muhammad Maaz, Hanoona Rasheed, Salman Khan, and Fahad Shahbaz Khan. Video-chatgpt:
666 Towards detailed video understanding via large vision and language models. *arXiv preprint*
667 *arXiv:2306.05424*, 2023.
- 668 Muhammad Maaz, Hanoona Rasheed, Salman Khan, and Fahad Khan. Videogpt+: Integrating image
669 and video encoders for enhanced video understanding. *arXiv preprint arXiv:2406.09418*, 2024.
- 670 Minesh Mathew, Dimosthenis Karatzas, and CV Jawahar. Docvqa: A dataset for vqa on document
671 images. In *Proceedings of the IEEE/CVF winter conference on applications of computer vision*,
672 pp. 2200–2209, 2021.
- 673 OpenAI. Openai gpt-3.5 api. *OpenAI API*, 2023a.
- 674 OpenAI. Gpt-4v(ision) system card. *OpenAI Blog*, 2023b. URL [https://openai.com/
675 index/gpt-4v-system-card/](https://openai.com/index/gpt-4v-system-card/).
- 676 OpenAI. Gpt-4 technical report. *ArXiv:abs/2303.08774*, 2023c. URL [https://arxiv.org/
677 abs/2303.08774](https://arxiv.org/abs/2303.08774).
- 678 OpenAI. Hello gpt-4o — openai. *OpenAI Blog*, 2024. URL [https://openai.com/index/
679 hello-gpt-4o/](https://openai.com/index/hello-gpt-4o/).
- 680 Adam Paszke, Sam Gross, Francisco Massa, Adam Lerer, James Bradbury, Gregory Chanan, Trevor
681 Killeen, Zeming Lin, Natalia Gimelshein, Luca Antiga, et al. Pytorch: An imperative style,
682 high-performance deep learning library. *Advances in neural information processing systems*, 32,
683 2019.
- 684 Viorica Patraucean, Lucas Smaira, Ankush Gupta, Adria Recasens, Larisa Markeeva, Dylan Banarse,
685 Skanda Koppula, Mateusz Malinowski, Yi Yang, Carl Doersch, et al. Perception test: A diagnostic
686 benchmark for multimodal video models. *Advances in Neural Information Processing Systems*, 36,
687 2024.
- 688 Charles R Qi, Or Litany, Kaiming He, and Leonidas J Guibas. Deep hough voting for 3d object
689 detection in point clouds. In *proceedings of the IEEE/CVF International Conference on Computer*
690 *Vision*, pp. 9277–9286, 2019.
- 691 Rui Qian, Xiaoyi Dong, Pan Zhang, Yuhang Zang, Shuangrui Ding, Dahua Lin, and Jiaqi Wang.
692 Streaming long video understanding with large language models. *arXiv preprint arXiv:2405.16009*,
693 2024.
- 694 QwenTeam. Qwen2 technical report. *arXiv preprint arXiv:2407.10671*, 2024a.

- 702 QwenTeam. Qwen2-vl: To see the world more clearly. *Wwen Blog*, 2024b. URL [https://](https://qwenlm.github.io/blog/qwen2-vl/)
703 qwenlm.github.io/blog/qwen2-vl/.
704
- 705 Alec Radford, Jong Wook Kim, Chris Hallacy, Aditya Ramesh, Gabriel Goh, Sandhini Agarwal,
706 Girish Sastry, Amanda Askell, Pamela Mishkin, Jack Clark, et al. Learning transferable visual
707 models from natural language supervision. In *ICML*, pp. 8748–8763. PMLR, 2021.
- 708 Mike Ranzinger, Greg Heinrich, Jan Kautz, and Pavlo Molchanov. Am-radio: Agglomerative vision
709 foundation model reduce all domains into one. In *CVPR*, pp. 12490–12500, 2024.
- 710 Ruchit Rawal, Khalid Saifullah, Ronen Basri, David Jacobs, Gowthami Somepalli, and Tom Gold-
711 stein. Cinepile: A long video question answering dataset and benchmark. *arXiv preprint*
712 *arXiv:2405.08813*, 2024.
- 713
714 Amanpreet Singh, Vivek Natarajan, Meet Shah, Yu Jiang, Xinlei Chen, Dhruv Batra, Devi Parikh, and
715 Marcus Rohrbach. Towards vqa models that can read. In *Proceedings of the IEEE/CVF conference*
716 *on computer vision and pattern recognition*, pp. 8317–8326, 2019.
- 717 Shengbang Tong, Ellis Brown, Penghao Wu, Sanghyun Woo, Manoj Middepogu, Sai Charitha
718 Akula, Jihan Yang, Shusheng Yang, Adithya Iyer, Xichen Pan, et al. Cambrian-1: A fully open,
719 vision-centric exploration of multimodal llms. *arXiv preprint arXiv:2406.16860*, 2024.
- 720
721 Haoning Wu, Dongxu Li, Bei Chen, and Junnan Li. Longvideobench: A benchmark for long-context
722 interleaved video-language understanding. *arXiv preprint arXiv:2407.15754*, 2024.
- 723
724 Junbin Xiao, Xindi Shang, Angela Yao, and Tat-Seng Chua. Next-qa: Next phase of question-
725 answering to explaining temporal actions. In *CVPR*, pp. 9777–9786, 2021.
- 726
727 Lin Xu, Yilin Zhao, Daquan Zhou, Zhijie Lin, See Kiong Ng, and Jiashi Feng. Pllava: Parameter-free
728 llava extension from images to videos for video dense captioning. *arXiv preprint arXiv:2404.16994*,
729 2024a.
- 730 Ruyi Xu, Yuan Yao, Zonghao Guo, Junbo Cui, Zanlin Ni, Chunjiang Ge, Tat-Seng Chua, Zhiyuan Liu,
731 Maosong Sun, and Gao Huang. Llava-uhd: an lmm perceiving any aspect ratio and high-resolution
732 images. *arXiv preprint arXiv:2403.11703*, 2024b.
- 733 Fuzhao Xue, Yukang Chen, Dacheng Li, Qinghao Hu, Ligeng Zhu, Xiuyu Li, Yunhao Fang, Haotian
734 Tang, Shang Yang, Zhijian Liu, et al. Longvila: Scaling long-context visual language models for
735 long videos. *arXiv preprint arXiv:2408.10188*, 2024.
- 736
737 Jingkan Yang, Yuhao Dong, Shuai Liu, Bo Li, Ziyue Wang, Chencheng Jiang, Haoran Tan, Jiamu
738 Kang, Yuanhan Zhang, Kaiyang Zhou, et al. Octopus: Embodied vision-language programmer
739 from environmental feedback. *arXiv preprint arXiv:2310.08588*, 2023a.
- 740 Jinyu Yang, Mingqi Gao, Zhe Li, Shang Gao, Fangjing Wang, and Feng Zheng. Track anything:
741 Segment anything meets videos. *arXiv preprint arXiv:2304.11968*, 2023b.
- 742
743 Yuan Yao, Tianyu Yu, Ao Zhang, Chongyi Wang, Junbo Cui, Hongji Zhu, Tianchi Cai, Haoyu Li,
744 Weilin Zhao, Zhihui He, et al. Minicpm-v: A gpt-4v level mllm on your phone. *arXiv preprint*
745 *arXiv:2408.01800*, 2024.
- 746 Alex Young, Bei Chen, Chao Li, Chengen Huang, Ge Zhang, Guanwei Zhang, Heng Li, Jiangcheng
747 Zhu, Jianqun Chen, Jing Chang, et al. Yi: Open foundation models by 01. ai. *arXiv preprint*
748 *arXiv:2403.04652*, 2024.
- 749
750 Qiying Yu, Quan Sun, Xiaosong Zhang, Yufeng Cui, Fan Zhang, Yue Cao, Xinlong Wang, and
751 Jingjing Liu. Capsfusion: Rethinking image-text data at scale. In *Proceedings of the IEEE/CVF*
752 *Conference on Computer Vision and Pattern Recognition*, pp. 14022–14032, 2024.
- 753 Xiang Yue, Yuansheng Ni, Kai Zhang, Tianyu Zheng, Ruoqi Liu, Ge Zhang, Samuel Stevens, Dongfu
754 Jiang, Weiming Ren, Yuxuan Sun, et al. Mmmu: A massive multi-discipline multimodal under-
755 standing and reasoning benchmark for expert agi. In *Proceedings of the IEEE/CVF Conference on*
Computer Vision and Pattern Recognition, pp. 9556–9567, 2024.

756 Xiaohua Zhai, Basil Mustafa, Alexander Kolesnikov, and Lucas Beyer. Sigmoid loss for language
757 image pre-training. In *Proceedings of the IEEE/CVF International Conference on Computer Vision*,
758 pp. 11975–11986, 2023.

759 Peiyuan Zhang, Kaichen Zhang, Bo Li, Guangtao Zeng, Jingkang Yang, Yuanhan Zhang, Ziyue
760 Wang, Haoran Tan, Chunyuan Li, and Ziwei Liu. Long context transfer from language to vision.
761 *arXiv preprint arXiv:2406.16852*, 2024a.

762
763 Ruohong Zhang, Liangke Gui, Zhiqing Sun, Yihao Feng, Keyang Xu, Yuanhan Zhang, Di Fu,
764 Chunyuan Li, Alexander Hauptmann, Yonatan Bisk, et al. Direct preference optimization of video
765 large multimodal models from language model reward. *arXiv preprint arXiv:2404.01258*, 2024b.

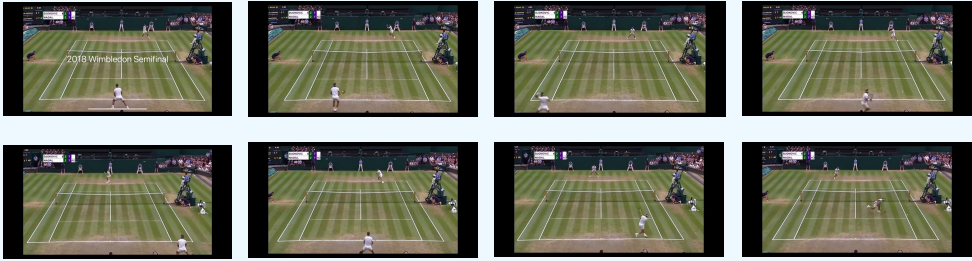
766
767 Yuanhan Zhang, Bo Li, haotian Liu, Yong jae Lee, Liangke Gui, Di Fu, Jiashi Feng, Ziwei Liu, and
768 Chunyuan Li. Llava-next: A strong zero-shot video understanding model, April 2024c. URL
769 <https://llava-vl.github.io/blog/2024-04-30-llava-next-video/>.

770 Junjie Zhou, Yan Shu, Bo Zhao, Boya Wu, Shitao Xiao, Xi Yang, Yongping Xiong, Bo Zhang,
771 Tiejun Huang, and Zheng Liu. Mlvu: A comprehensive benchmark for multi-task long video
772 understanding. *arXiv preprint arXiv:2406.04264*, 2024.

773
774
775
776
777
778
779
780
781
782
783
784
785
786
787
788
789
790
791
792
793
794
795
796
797
798
799
800
801
802
803
804
805
806
807
808
809

810
811
812
813
814
815
816
817
818
819
820
821
822
823
824
825
826
827
828
829
830
831
832
833
834
835
836
837
838
839
840
841
842
843
844
845
846
847
848
849
850
851
852
853
854
855
856
857
858
859
860
861
862
863

Video Summarization and Detailed Description




User: Describe what is happening in the video in detail.

Oryx: The video captures a moment from the 2018 Wimbledon Semifinal between **Djokovic and Nadal**. The scene is set on a grass court, with the players positioned on opposite sides of the net. Djokovic, dressed in white, is seen preparing to hit the ball, while Nadal, also in white, is poised to return the shot. The scoreboard indicates that the match is **tied at 7-7, adding to the tension of the moment**. ...

LLaVA-OneVision: The video begins with a wide shot of a grass tennis court during the 2018 Wimbledon Semifinal. Two players, both dressed in white, are positioned on either side of the net. The player on the left is preparing to serve, while the player on the right is ready to return. The court is surrounded by a large audience, and the scoreboard in the background shows the names **'SACHSNOVIC' and 'DRAKOVIC'** with scores.

Figure 4: Oryx is able to make a comprehensive video summary and detailed caption.

Video Multiple Choice and Reasoning



User: According to the video, if I have some expired aspirin, which kind of waste is it?
A. Waste. B. Toxic Waste. C. Wet or Organic Waste. D. Dry waste.

Oryx: **The answer is B**, because expired aspirin is a kind of drug, drugs are toxic waste. The video explains that if you have some expired aspirin, **it is considered toxic waste**. This is because drugs can be harmful to the environment and should not be disposed of in the regular trash. Instead, they should be taken back to a pharmacy or other designated location for proper disposal.

LLaVA-OneVision: Expired aspirin is categorized as toxic waste, as indicated in the video. Toxic waste includes substances like medicines, which need special care when disposing of them to prevent environmental and health risks. **Therefore, the correct answer is B**. Toxic Waste. It's important to dispose of such items properly, often through designated hazardous waste disposal facilities or special collection events.

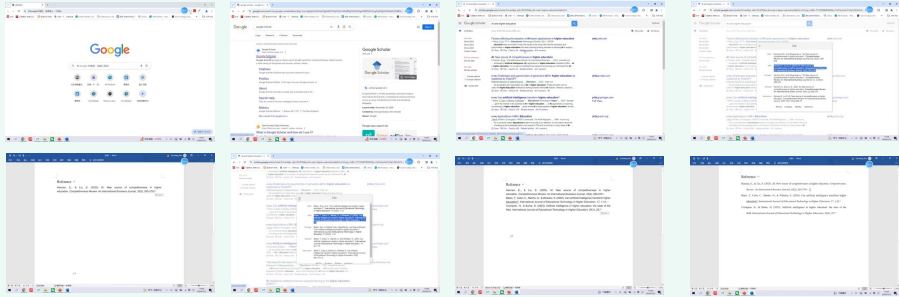
Figure 5: Oryx learns to reason through the input video.

A GENERATION RESULTS

Video Summarization and Detailed Description. As shown in Fig. 4, the Oryx model effectively generates a comprehensive and detailed caption that accurately summarizes the input video. It captures the main event while preserving essential information. **Oryx produces more accurate results about the match information, the name, and the status of the player.** In contrast, LLaVA-OneVision (Li et al., 2024a) shows the wrong name, and LongVILA tells the wrong score on the board.

864
865
866
867
868
869
870
871
872
873
874
875
876
877
878
879
880
881
882
883
884
885
886
887
888
889
890
891
892
893
894
895
896
897
898
899
900
901
902
903
904
905
906
907
908
909
910
911
912
913
914
915
916
917

Skill Learning From Videos




User: According to the video, if I want to cite the paper titled 'Oryx', what should I do? List the actions below.

Oryx: To cite the paper titled 'Oryx', you should follow these steps: 1. Open google chrome and search for google scholar. 2. Search for **the paper 'Oryx'**. 3. Select the paper from the search results and **click on the "Cite" button** to generate the citation in your preferred format. 4. Copy the generated citation and paste it into your document where you want to reference the paper.

LLaVA-OneVision: To cite the paper titled 'Oryx' from the video, follow these steps: Open the Google Scholar webpage and search for the paper 'Oryx'. Once you find the paper, **click on the three dots next to it** and select 'Cite'. Choose the citation format you need, **such as APA, MLA, or Chicago**. If the paper's details are not automatically filled, **manually input the information from the paper's publication details including authors, title, year, and journal**. Copy the citation and paste it into your bibliography or reference list.

Figure 6: Oryx learns useful skills from the input video.

Understanding 3D with Coarse Correspondences



User: If Alice comes out of the building and wants to go down the stairs and cross the street using the pedestrian crossing, which direction should she turn after exiting the door?
A. Left B. Right.
Please answer from Alice's perspective, not the observer's. Explain why using the labels inside the images.

Oryx: If Alice comes out of the building and wants to go down the stairs and cross the street using the pedestrian crossing, she should **turn right after exiting the door**. This is because the pedestrian crossing is located on the right side of the entrance when facing it from inside the building. The labels inside the images indicate that the pedestrian crossing (label 3) is to the right of the door (label 4), and the stairs (label 1) are also situated to the right of the door when viewed from Alice's perspective. Therefore, turning right would lead Alice towards the pedestrian crossing and then across the street.

LLaVA-OneVision: After exiting the door, Alice should **turn left**. This is because..., as indicated by the position of the yellow fire hydrant (label 1) and the bicycle rack (label 2) in the images. Turning left will lead her towards these features and ultimately to the street where she can use the pedestrian crossing.

Figure 7: Oryx understands 3D spatial information through coarse correspondences.

Video Multiple Choice and Reasoning. Oryx is also capable of reasoning based on the input video. As demonstrated in Fig. 5, Oryx can answer questions through analogy and generate well-reasoned responses.

Skill Learning From Videos. Oryx can acquire useful skills from the input video. As demonstrated in Fig. 6, Oryx learns to use Google Scholar to cite a paper by following the steps shown in the video. It illustrates all the necessary steps to complete the citation, highlighting its strong skill-learning capability and potential for agent-based tasks and task execution. **Although the baseline model**

918
919
920
921
922
923
924
925
926
927
928
929
930
931
932
933
934
935
936
937
938
939
940
941
942
943
944
945
946
947
948
949
950
951
952
953
954
955
956
957
958
959
960
961
962
963
964
965
966
967
968
969
970
971

Video Time Perception

User: Describe what happened at 15-18 seconds. Describe the scene in detail.

Oryx: At 15-18 seconds, the video captures a moment during the 2018 Wimbledon Semifinal between Novak Djokovic and Rafael Nadal. The scene is set on a grass court with players positioned on opposite sides of the net. The scoreboard in the background shows that the match is tied at 7-7, indicating a closely contested game. The player on the left side of the court is preparing to hit the ball, while his opponent on the right side is anticipating the shot. The audience in the stands is visible, adding to the atmosphere of the event. **(The answer is wrong. in 15-18 seconds, djokovic wins the point with a forehand shot.)**

Figure 8: Failure cases about time perception.

Knowledge Reasoning and Transfer

User: What is the purpose of beating the balloon? Describe in detail.

Oryx: The purpose of beating the balloon is to create a series of air pockets within it. This process involves repeatedly striking the balloon with a flat, blunt object, such as a wooden spoon or a similar tool, until it becomes visibly deflated and has multiple air pockets throughout its surface. The air pockets are created by the impact of the object on the balloon's surface, causing the air inside to be released and trapped in the form of bubbles. **(The answer is wrong. The correct purpose is to conduct chemical reaction and generate the cute globefish.)**

Figure 9: Failure cases about knowledge reasoning and transfer.

provides additional instructions, some detailed steps are not depicted in the original video. We believe this hallucination may stem from the information in the training data.

Understanding 3D with Coarse Correspondences. Oryx enhances its 3D spatial understanding using coarse correspondences. Fig. 7 illustrates Oryx’s reasoning process, demonstrating its ability to improve 3D comprehension through these correspondences and generate accurate reasoning outcomes. In the challenging task involving direction in a first-person view, LLaVA-OneVision (Li et al., 2024a) provides incorrect conclusions.

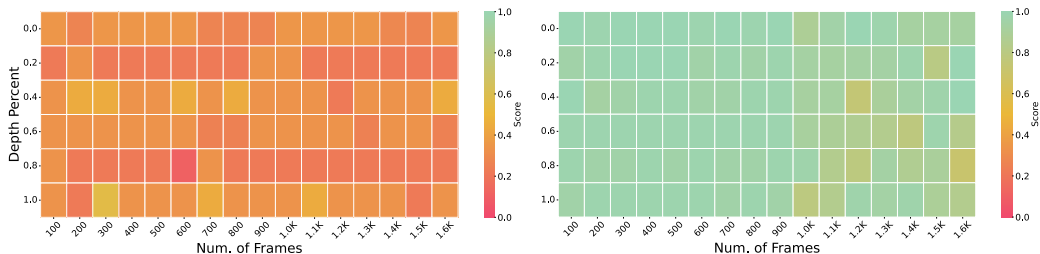


Figure 10: **Visualization Results on Video Needle-In-A-Haystack Experiments.** We compare Oryx-7B (right subfigure) with LLaVA-Next-Video-7B (left subfigure) on the frame retrieval task. The results are shown for inserted depths ranging from 0.0 to 1.0 and the number of frames ranging from 0.1k to 1.6k. The Oryx model demonstrates superior performance in long-form understanding tasks, providing precise results even when a single relevant frame is embedded within over 1k frames of irrelevant information.

B FAILURE CASES

In this section, we further test the Oryx model on more challenging samples. We provide some representative failure cases to show the limitations of the Oryx model and point out the future direction for VLMs. The incorrect response is highlighted in red.

Time Perception. We provide an example of time perception in Fig. 8. From the responses, we can observe that current video understanding models using uniform frame sampling tend to lose the temporal context in videos, which is critical information between frames. For instance, Oryx provides incorrect answers and cannot accurately determine the timestamps for the given video. We believe that incorporating timestamps directly into the video or processing video inputs without frame sampling may help address this issue, leading to a more comprehensive video understanding capability.

Knowledge Reasoning and Transfer. We provide the knowledge reasoning video in Fig. 9. From the responses, we can observe that the Oryx model lacks knowledge of chemical reactions, indicating that the training data of current MLLMs is not comprehensive enough. We believe that expanding the knowledge base of current MLLMs is an urgent issue. Additionally, this example requires simple reasoning to integrate chemical knowledge into the main idea of the video, which poses a challenge for Oryx. Enhancing the reasoning capability may help address this issue.

C MORE ANALYSIS

C.1 VIDEO NEEDLE-IN-A-HAYSTACK

To demonstrate the retrieval ability in long-form visual inputs and test the quality of the dynamic compression module, we design the video needle-in-a-haystack experiment under extreme conditions, following the methodologies established in previous work (Zhang et al., 2024a; Xue et al., 2024). For this experiment, we select an extremely long video and then insert irrelevant image question-answering data as a single frame at arbitrary depths within the video. The model is tasked with answering questions related to these inserted images. We utilize LLaVA-Next-Video (Zhang et al., 2024c) of comparable size as our baseline. As depicted in Figure 10, baseline models trained with 32 frames failed to identify the images, suffering from severe information loss. In contrast, our method successfully retrieves the inserted images and accurately answers the questions, even with frame counts of 1.6k. This outcome strongly demonstrates the model’s ability in long-form temporal understanding, facilitated by the on-demand compression module.

C.2 INFERENCE SPEED AND EFFICIENCY

We implement variable-length self-attention using the highly optimized FlashAttention (Dao et al., 2022) library. This allows the inference throughput of our arbitrary-resolution visual encoder to

1026
1027
1028
1029
1030
1031
1032
1033
1034
1035
1036
1037
1038
1039
1040
1041
1042
1043
1044
1045
1046
1047
1048
1049
1050
1051
1052
1053
1054
1055
1056
1057
1058
1059
1060
1061
1062
1063
1064
1065
1066
1067
1068
1069
1070
1071
1072
1073
1074
1075
1076
1077
1078
1079

Table 6: **Test on Inference Speed and Memory Cost.**

Backbone	Processing Approach	Throughput (image/s)	Max Memory Cost
OryxViT	Native Resolution	146.5	49.1GB
SigLIP	Dynamic Partition	157.7	48.7GB

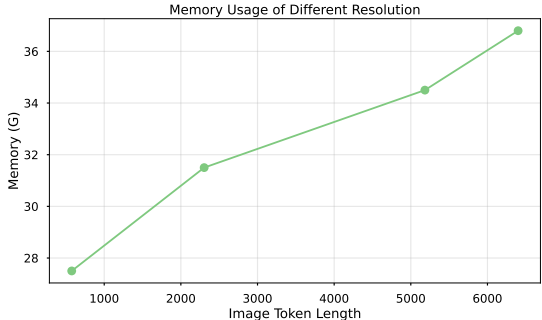


Figure 11: **Memory-Resolution Curve for OryxViT.**

remain comparable to the dynamic partition approach used in previous methods. Additionally, the memory overhead and inference throughput remain negligible, as the variable-length attention operation is fully optimized through modifications in the CUDA kernels.

Moreover, the model size of the Vision Transformer is considerably smaller than that of large language models (400M parameters compared to 7B/32B). Consequently, the main memory cost arises from the weights and features of the LLMs, as full attention is computed on visual tokens within the LLM, even when using dynamic partitioning in visual encoding. Therefore, we maintain a similar efficiency to previous solutions in terms of inference speed and memory cost.

We tested the inference speed with an input image size of 1280×1280 on one NVIDIA A100 GPU. We observed that OryxViT is only 7% slower than SigLIP with the dynamic partition approach. We believe this overhead is acceptable given the improved performance and the ability to process images at their native resolutions directly. For the max memory cost, we set the batch size to 4 and the image size to a total of 1280×1280 pixels, with the aspect ratio randomly determined. The dynamic-partition baseline uses an average of 48.7G of memory, while OryxViT uses 49.1G, showing comparable results.

Additionally, we plotted the memory-resolution curve to illustrate how the memory footprint increases with varying resolutions in Fig. 11. Our experiment was conducted on an NVIDIA A100 GPU, using square-shaped input images. The results show that the memory cost is positively correlated with image resolution and is approximately in linear relation among common image resolutions, indicating that OryxViT provides a memory-efficient solution when scaling input resolutions.

Furthermore, we can also observe that the primary memory cost arises from the model weights and the features themselves. Notably, considering that the main memory cost comes from the computation in LLMs, our method with native resolution support will not introduce much extra memory footprint compared to previous methods like LLaVA-Next (Liu et al., 2024c) and InternVL2 (Chen et al., 2024b). Oryx can largely save memory if we apply dynamic compression on visual tokens (e.g., 2x or 4x downsampling) while previous methods do not support this feature.

C.3 ABLATIONS ON TRAINING DATA

We conduct ablation experiments on the collected training data including the long-form video data and the 3D coarse corresponding data in Tab. 7. We can observe from the results that the long-form temporal data benefits the long video benchmarks. For 3D-related tasks, our proposed approach based on coarse correspondence is an effective solution for 3D benchmarks. We conducted experiments and provided results on ScanQA. "3D Data" indicates whether 3D datasets are included in the training set,

Table 7: **Ablations on Training Data.**

(a) Effects on Long-Form Data.			(b) Effects on 3D-relevant Data.			
Long-Form Data	VideoMME	MLVU	3D Data	C.C.	METEOR	ROUHE-L
\times	55.2	58.1	\times	\times	11.7	28.1
\checkmark	55.4	59.3	\checkmark	\times	12.8	32.7
			\checkmark	\checkmark	14.0	35.1

Table 8: **Ablations on Designs of MLP Adapter.**

MLP Architecture	VideoMME	MLVU	MMBench	MMMU
Shared	55.4	59.3	81.4	43.9
Separated	54.0	54.2	81.2	43.1

while "C.C." refers to using the coarse correspondence approach to annotate objects in 3D-relevant videos. We observe that both components contribute to an improved understanding results.

C.4 DESIGNS FOR MLP ADAPTER

We explored using specialized projection layers when integrating video modality into our model. However, we found that employing a shared MLP for all visual inputs yields better performance. To align with this design, we use the Dynamic Compressor module to closely maintain the distribution of image and video features and employ the shared MLP for visual information fusion. This ensures that input tokens for LLMs maintain a consistent distribution for both images and videos, allowing the shared MLP to be better trained with joint visual knowledge.

We conducted experiments in Tab. 8 to support our hypothesis, comparing our shared MLP strategy with separate MLPs for images and videos. Both the image and video MLPs were initialized from pre-trained image weights. The results indicate that using separate MLPs negatively impacts video benchmarks, as the dual-projector design can lead to differing distributions for similar data. Therefore, using a single MLP is a more effective solution for visual encoding.

C.5 ANALYSIS ON DOWNSAMPLING

Analysis on Overall Downsampling Architecture. We integrate several mainstream approaches, including direct average pooling, 2×2 spatial convolution, Q-former, and our proposed Dynamic Compressor for comparison. The results are presented in Tab. 9 (a). We reference results from VideoMME (Fu et al., 2024) and MLVU (Zhou et al., 2024). Our observations indicate that the proposed Dynamic Compressor outperforms traditional downsampling strategies based on average pooling and spatial convolution. Additionally, we find that Q-former-based methods are not suitable for handling long visual content with fixed lengths of visual tokens. This limitation arises because the information capacity of a visual token is directly proportional to its length, making fixed lengths inadequate for more complex cases involving longer visual content.

Analysis on Downsampling Function in Dynamic Compressor We are also curious which downsampling function performs better within the dynamic compressor. We compared average pooling, DWConv, and Conv-MLP architectures. The results are presented in Tab. 9 (b). Results indicate that the parameter-free average pooling outperforms parameter-dependent methods like DWConv and Conv-MLP. This improvement is likely because average pooling better preserves the distribution of visual features, whereas more complex downsampling layers may not be effectively trained with the current pipeline.

Table 9: **Analysis on Downsampling.**

(a) Overall Downsampling Architecture.			(b) Downsampling Function in Dynamic Compressor.		
Strategy	VideoMME	MLVU	Function	VideoMME	MLVU
Average Pooling	54.6	57.5	DWConv	55.0	58.9
Convolution	54.2	56.8	Conv-MLP	54.7	58.5
Q-former	42.7	35.3	Average Pooling	55.4	59.3
Dynamic Compressor	55.4	59.3			

D MORE DETAILS

D.1 IMPLEMENTATION DETAILS

Our implementation integrates the Oryx model with two sets of LLMs, Qwen-2.5-7B (QwenTeam, 2024a), and Yi-1.5-34B (Young et al., 2024), to demonstrate generalizability across different model sizes. For the visual encoder, we use our pre-trained OryxViT to support arbitrary-resolution visual inputs. During the pre-training stage, we utilize 558k captioning data from LLaVA-1.5 (Liu et al., 2024b), unfreezing the parameters of the dynamic compression module. The image SFT stage involves curating an open-source dataset of around 4M images. In the joint training stage, we incorporate approximately 1.2M data consisting of images sampled from the previous stage and video/3D data. For video data, we restrict the frame number to 64 for standard videos of low compression ratio and 256 for long videos of high compression ratio. We use the 2×2 average downsample for low compression and 4×4 average downsample for high compression. Image data are maintained at their native resolution, with a maximum size of 1536 pixels, while video data resolutions are confined to a range of 288 to 480 pixels. The rest of the training details are provided in the appendix. In our implementation, we set the downsampling ratio $d_3 = 4d_2 = 16d_1$, therefore the token length of frames in the long videos is reduced to $\frac{1}{16}$ of that of images with the same resolution.

D.2 DETAILS OF ORYXViT

We pre-train OryxViT with a relatively small language model (Qwen2-0.5B (QwenTeam, 2024a) in our implementation) to enhance the language interface and improve vision-language alignment. We unfreeze OryxViT and apply LoRA fine-tuning to the language models. As a result, the total number of trainable parameters is 0.6B, making the training process significantly faster than supervised fine-tuning in the main stage (approximately 10 times faster). We collected a total of 400M pre-training data, focusing mainly on image captioning and image OCR tasks. For image captioning, we used the CapsFusion (Yu et al., 2024) datasets, and for OCR tasks, we employed synthesized OCR data pairs with OCR models. We set the batch size to 2048 and used a similar cross-entropy loss as in the main stages.

D.3 TRAINING DETAILS

Stage 1. For stage 1, we first pre-train the connector module between the visual encoder and Large Language Model for the initial alignment between image and text modalities. We conduct our experiments on 558k caption data from BLIP (Li et al., 2023) model following LLaVA-1.5 (Liu et al., 2024b). We only unfreeze the parameter for the connector while maintaining other parameters fixed. We adopt the total training batch size at 256 and the overall learning rate at $1e-3$. We maintain the aspect ratio for the input image while adjusting the overall pixels to 768^2 to reduce the computational cost. The training cost for the pre-training alignment is lightweight thanks to the small number of parameters for the connector and the relatively lower image-text data pairs. Subsequently, we conduct the supervised fine-tuning stage with 4.1M image data. We freeze the parameter for the visual encoder while unfreezing the connector and the Large Language Model following common practice. In this stage, we use the native resolution of the image while restricting the maximum number of pixels at 1280^2 for efficiency. For the image larger than 1280^2 pixels, we scale down the image to match the overall number of pixels. We set the learning rate at $2e-5$ for Oryx-7B and the learning rate at $1e-5$ for Oryx-34B. We adopt the total batch size at 128 and conduct our experiments on 64 NVIDIA

1188 A100-40G GPUs for Oryx-7B and 64 NVIDIA A800-80G GPUs for Oryx-34B, as larger models
1189 need more GPU memories. The total model maximum length is set as 8192.
1190

1191 **Stage 2.** For stage 2, we continuously train the Oryx model from the multi-modal LLMs in stage
1192 1. We randomly sample around 600k image data from the supervised fine-tuning stage in stage 1
1193 and add an additional 650k temporal and 3D data from open-source multi-modal datasets, resulting
1194 in an overall number of 1.2M further supervised fine-tuning data. In the more general stage, we
1195 increase the restriction for image pixels to 1536^2 to meet the longer sequential length in temporal
1196 data. We maintain the aspect ratio of video data while normalizing each frame to the minimum size of
1197 288^2 pixels and the maximum size of 480^2 pixels, therefore the token length before the compression
1198 module ranges from 324 to 900. We adopt 1×1 path for the image data, 2×2 pooling path for the
1199 multi-frame data including video and 3D-relevant data, and 4×4 pooling path for the extremely
1200 long video needle-in-the-haystack retrieval data. We maintain most of the training hyper-parameters
1201 identical to stage 1, with a total batch size of 128, a learning rate of $2e-5$ for Oryx-7B, and a learning
1202 rate of $1e-5$ for Oryx-34B. We sample 1 frame per second for video data and set the max frame
1203 number at 64 frames. We uniformly sample the frames among all the frames if the number exceeds
1204 the upper bound. The maximum sequence length is set to 16384.

1205 E CODE

1206
1207 The code is also provided in the supplementary material (see the `code` folder). Our Oryx is
1208 implemented using PyTorch library (Paszke et al., 2019).
1209
1210
1211
1212
1213
1214
1215
1216
1217
1218
1219
1220
1221
1222
1223
1224
1225
1226
1227
1228
1229
1230
1231
1232
1233
1234
1235
1236
1237
1238
1239
1240
1241